A Particle-in-Cell Simulation of Dust Charging and Shielding in Low Pressure Glow Discharges

Seung J. Choi, *Member, IEEE*, and Mark J. Kushner, *Fellow, IEEE*

Abstract—**The transport of particles ("dust") in low pressure electrical glow discharges is being studied in regard to its role in contaminating silicon wafers during plasma etching and deposition. Particles (10s nm–μm) negatively charge in glow discharges and, to first order, appear to be massively large negative ions around which sheaths develop. The forces on particles in plasmas include electrostatic (drift of charged particles in electric fields) and viscous ion drag. The latter force is momentum transfer from ions to particles by either collisions or orbital motion. This force critically depends on the charge on the particle and the shape of the sheath surrounding the particle. In this work, we report on a Pseudoparticle-in-Cell (PIC) simulation of the transport of electrons and ions in the vicinity of dust particles in low pressure glow discharges. The simulation produces the electrical charge on the dust particle, the sheath structure around the dust particle and the orbital dynamics of the ions. A companion molecular dynamics simulation uses these parameters to produce ion-dust and electron-dust particle cross sections for momentum transfer and collection. Results will be discussed for charge, sheath thickness, cross sections and viscous ion drag forces on dust particles as a function of radius and plasma parameters.**

I. Introduction

THE contamination of plasma etching and deposition electrical discharges by particles ("dust") is problematic due to reduced yields of the products and perturbation of the plasma. These particles are 10s nm to 10s μm in size. A number of studies have been recently performed to investigate the transport and accumulation of particles in plasmas, and radio frequency (RF) discharges in particular. Roth and Spears first used laser light scattering to observe that particles accumulate in RF discharges near the bulk plasma-sheath boundary [1]. Subsequent observations by Selwyn *et al.* [2]–[4], Graves *et al.* [5]–[7] and Watanabe *et al.* [8]–[9] confirmed these observations in a variety of dc and RF discharges, for different gas mixtures and particle compositions. A common observation is that large particles ($> 0.1\,\mu$m) accumulate near the sheath edge, while small particles accumulate in the center of the discharge at the location of the maximum in the plasma potential. Selwyn *et al.* [3] and Carlisle *et al* . [10] also observed that particles accumulated at the sheath-plasma boundary in rings around semiconductor wafers and domes above the wafers in etching RF discharges.

These observations demonstrate that particles which have different compositions in different types of discharges using different gas mixtures behave similarly. This suggests that the transport of particles depends largely on fundamental plasma properties and not on the details of the plasma chemistry or excitation mechanisms. All of these observations are also consistent with the particles being negatively charged.

Sommerer *et al.* [11] and Barnes *et al.* [12] have proposed that transport of small particles (when gravity is not important) is dominated by two forces; electrostatic and viscous ion drag. The former force accelerates negatively charged particles towards the center of electropositive plasmas or towards local maxima in the plasma potential. The latter force accelerates particles in the direction of net ion flux, which is generally towards the boundaries of the plasma. Ions, attracted towards the negatively charged particles, perform open orbit trajectories around the particle. To conserve momentum, the particle is accelerated in the direction of the original ion motion. In low electric fields, as in the bulk plasma, the viscous ion drag force exceeds the electrostatic force and the particles are accelerated towards the boundaries of the plasma. In large electric fields, as found in the sheath regions near surfaces or electrodes, the electrostatic force exceeds the ion drag force and the particles are forced into the plasma. The particles accumulate where these forces balance, which is typically at the edge of sheaths. The viscous ion drag force scales more strongly with radius of the particle than does the electrostatic force. Therefore, for larger particles, the electrostatic and ion drag forces balance further into the high electric field regions of sheaths. In a similar fashion, sufficiently small particles are forced to the center of the plasma by electrostatic forces where the plasma potential is usually most positive.

Recently, however, electric probe measurements of the plasma potential in RF discharges have revealed that particles are commonly found in positive potential traps (perhaps as large as 7 V) which are observed coincident with the accumulation of the particles [13]. There is evidence that these potential traps may predate the accumulation of particles, although it is not clear if the particles actually grow in the traps. Regardless, the transport of particles which are formed elsewhere in the plasma to these traps can be adequately explained by ion drag and electrostatic forces. Under certain conditions, thermophoresis, polarization and neutral fluid viscous forces may also influence the transport of particles in low pressure plasmas [5]–[7], [14].

Manuscript received July 8, 1993; revised October 7, 1993. This work was supported by the National Science Foundation, Sandia National Laboratory, IBM East Fishkill Facility, and the Semiconductor Research Corporation.

S. J. Choi was with the Department of Electrical and Computer Engineering, University of Illinois, Urbana, IL 61801. He is now with Sandia National Laboratories, Albuquerque, NM 87185.

M. J. Kushner is with the Department of Electrical and Computer Engineering, University of Illinois, Urbana, IL 61801.

IEEE Log Number 9215634.

There is ample evidence that small gradients in electrostatic forces are sufficient to alter the locations in which particles accumulate. For example, Selwyn *et al.* [15] machined grooves in the electrodes surrounding semiconductor wafers in an RF etching discharge. This formed a local minimum in the physical height of the plasma-sheath boundary, and so generated a small radial electric field pointing from the center of the wafer towards the groove. Particles which are trapped in the axial direction at the plasma-sheath boundary as a result of there being a balance between ion drag and electrostatic forces, can move towards and accumulate in the grooves under the influence of a small radial field. Due to the sign of the radial electric field, the particles were most likely forced towards the grooves by ion drag.

The shielding of particles plays an important role in all of the forces discussed above with the exception of gravity. The shielding and charging of dust particles has been studied extensively in the context of dusty plasmas in the interplanetary and interstellar media [16]–[18]. Our conditions are quite different than those of space plasmas. In particular, our plasma densities are larger ($10^{10} - 10^{12}\,\mathrm{cm}^{-3}$), particle densities are larger ($10^5 - 10^8\,\mathrm{cm}^3$), and our ratio of Debye length to particle spacing is typically much less than unity. The collisionality of plasma processing discharges is also greater than space plasmas, thereby altering electron and ion energy distributions from Maxwellians; and perturbing their trajectories. Nevertheless, there are strong similarities between dusty plasmas in space and in plasma processing. Dust particles charge negatively in plasmas to ensure that the flux of more mobile electrons to their surface does not exceed that of the heavier and, in most cases, cooler ions. Dust particles having diameters of 10 s nm to many microns appear to be massively large negative ions having many hundreds to thousands of charges; and charge to a few times the electron temperature. They have a low mobility compared to the lighter singly charged positive ions. For these conditions, positive ions shield the large heavy negatively charged particles in a similar fashion as light electrons may shield heavy positive ions. The details of the sheath structure, particle potential, and ion density in the vicinity of the particle are therefore important in determining the relative magnitudes of the ion drag and electrostatic forces.

The sheath properties of particles in plasmas, and the resultant forces have been theoretically addressed by Barnes *et al.* [12] and Graves *et al.* [19]–[21]. In these works electrostatic and ion drag forces on the particles were investigated using semianalytic theories. In particular Graves *et al.* used the linearized Debye length, λ_L, to characterize the shielding of particles by both electrons and ions. For conditions where the diameter of the dust particle, d, is much less than λ_L, the shielding distance is a fraction of λ_L. As d/λ_L increases, the shielding distance also increases, a consequence of there being a smaller component of orbital motion around the particle. In both of the cited works, the particle potential (with respect to the plasma potential far from the particle) is predicted to be approximately $-2 \cdot T_e$(T_e is the electron temperature).

McCaughey and Kushner examined the effects of particles on the electron energy distribution (EED) using a Monte Carlo simulation, and found that the large momentum transfer cross sections represented by the dust particles damped the EED [22], [23]. Increasing the dust density at constant electric field reduced the electron impact rate coefficients for high threshold events, such as ionization. These results were later used in a numerical model for cylindrical glow discharges by appropriately modifying the electron transport coefficients in the presence of dust [24]. Higher self-sustaining electric fields were predicted at higher dust densities or larger particle sizes.

Boeuf numerically modeled the flow of current through an argon dusty plasma using a pseudoparticle-in-cell simulation [25]. His particles were cylindrical and uniformly spaced. In this work, the distortion of the electron and ion distribution functions as a function of position are explicitly obtained. By requiring that the time averaged rate of electron production and loss be the same, a self-consistent voltage across the plasma was calculated. He found that the self-sustaining electric field generally increased with increasing particle size, as did the electron temperature, to compensate for the loss of charge to the dust particles which act as recombination centers.

In this paper, we describe and present results from a pseudoparticle-in-cell computer simulation of the charging and shielding of dust particles in low temperature plasmas. (To avoid confusion, the computational electron and ion particles used in the simulation will be called pseudoparticles. Contaminating particulates in the plasma will be called dust particles.) In this model, electron and ion energy distribution functions and densities are obtained in the vicinity of the dust particles while solving Poisson's equations for the electric field. The electron and ion pseudoparticles undergo both neutral and coulomb collisions, and are collected on the particle. The results of the model provide the shielding distances, the effective momentum transfer cross sections of the dust particle, and the magnitudes of the ion drag forces. The model is described in Section II. A discussion of our results for shielding properties appears in Section III, and a discussion of calculated electron- and ion-dust cross sections appears in Section IV. Our concluding remarks are in Section V.

II. Description of the Model

The model is a Pseudoparticle-in-Cell/Monte Carlo Collision (PIC/MCC) simulation for electrons and ions in the vicinity of a dust particle. (The terminology Pseudoparticle-in-Cell is used to avoid confusion between numerical particles and dust particles). The PIC/MCC simulation is performed in a cubic volume $10\mathrm{s} - 100\mathrm{s}\,\mu\mathrm{m}$ on a side using periodic boundary conditions. (See Fig. 1). Within this volume is a spherical subvolume at the center of which a dust particle is placed. Poisson's equation for the electrical potential is solved within the spherical subvolume. Electron or ion pseudoparticles pass freely between the spherical subvolume and the remainder of the cubic computational volume. The only distinction between the two regions is that we solve Poisson's equation within the spherical subvolume while we assume quasineutrality outside the subvolume. The radius of the subvolume was chosen to be sufficiently large to enclose the entire dust particle

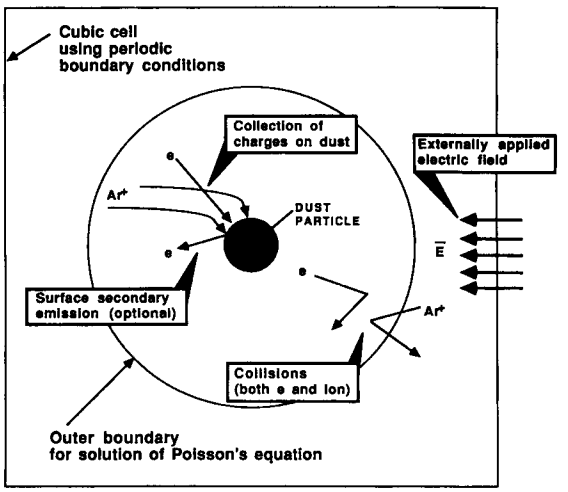

Fig. 1. Schematic of the PIC-MCC simulation. The dust particle is placed at the center of a spherical region in which Poisson's equation is solved. The computational region is bounded by a cube with which periodic boundary conditions are used.

shielding region. The boundary condition on the surface of the spherical subvolume and on the boundaries of the cube is $\vec{\nabla}\phi/N = -\vec{E}/N$, where ϕ is the electric potential, E is the specified bulk electric field, and N is the gas density.

The simulation begins by specifying a gas mixture and an applied E/N to the bulk plasma. (E/N is a scaling parameter for the strength of electric fields in low temperature plasmas. Typical values are $0.1 - 10 \times 10^{-17}\,\mathrm{V} - \mathrm{cm}^2$.) Conventional Monte Carlo simulations for electrons and ions are performed in a uniform electric field in the absence of the dust particles to obtain self consistent electron energy distributions (EED's) and ion energy distributions (IED's) far from the particle. A description of the Monte Carlo methods used in this study can be found in [26]. These distributions then serve as initial conditions for the PIC/MCC including the dust particle. After obtaining the initial EED and IED based on the uniform E/N, a dust particle having a specified radius is placed at the center of the spherical subvolume and a solution of Poisson's equation is added to the simulation. The electron and ion psuedoparticles are advanced using a second order Runga Kutta technique in the self-consistent electric fields for $\Delta t \approx 5 \times 10^{-12} - 10^{-11}\,s$ between solution of Poisson's equation. The actual time steps for the individual electron and ion pseudoparticles are individually chosen based on their velocity, acceleration, position on the mesh, and the time to the next collision. This allows the ion and slow electron pseudoparticles to be moved less frequently than the more energetic electrons, and is a de facto "sub-cycling" technique.

The time step for each pseudoparticle is the minimum of the time to the next collision, the time required to cross a specified fraction of the local computational cell or the time to the next update of the electric field. In practice, the electric field is interpolated for a given pseudoparticle's position from the spherical mesh upon which Poisson's equation is solved. As a pseudoparticle approaches the dust particle and $\nabla|E|$ increases, the time step must be further constrained to prevent numerical heating. This is accomplished by reducing the fraction of the computational mesh which the particle may traverse in a given time step. Pseudoparticles are typically moved only 0.5 of a cell dimension on any given update. Near the particle, the pseudoparticles are moved only 0.1 of the mesh spacing.

The simulation uses a spherical 2-D (r, Θ) mesh in the subvolume upon which Poisson's equation is solved. The inner radius of the mesh sits on the surface of the dust particle, the outer radius is on the outer surface of the spherical subvolume. For a dust particle 1 μm in radius, the mesh spacing decreases from $\approx$0.1 μm far from the surface of the particle to as small as $\approx$0.01 μm near the dust particle. The mesh spacing is constant but smaller in successively smaller spherical subvolumes. The mesh spacing decreases with decreasing radius of the dust particle to resolve the large value of $\nabla|E|$ near the dust particle.

When the mesh spacing is small near the dust particle, the statistics for the charge collected on the numerical mesh are poor, while the values of $\nabla|E|$ are large. Under these conditions, particularly for small dust particles ($<$1 μm) we found that the solution of the electric field was often constrained by the mesh spacing. For parametric purposes, the inner radius of the mesh was displaced from the surface of the dust particle. The electric potential was analytically calculated in the gap between the surface of the dust particle and the inner radius of the numerical mesh. The analytic and numerical solutions were then matched at the boundary. This technique was adequate to approximate the charge on the particle for use as initial conditions for a full solution.

The solution of Poisson's equation includes the net electrical charge both in the plasma and on the surface of the dust particle. Charge in the plasma appears on the right hand side of Poisson's equation in the conventional way. In the PIC simulation all charge collected in a cell was placed at the cell center. Pseudoparticles which collide with the dust particle are removed from the simulation, and their charge is added to the charge on the surface of the dust particle. The surface charges are used to formulate a boundary condition for the potential at the surface of the dust particle for use in Poisson's equation.

$$-\nabla\phi(\Theta) = \frac{\sigma(\Theta)}{\epsilon_0} \tag{1}$$

where σ is the surface charge density and Θ is the polar coordinate on the dust particle.

In the context of this work, we attempted to differentiate between dielectric and metallic particles by the charge distribution on the surface of the dust particle. For a metallic particle the boundary condition is $E_{||} = 0$, and $\sigma(\Theta)$ is constant. Under these conditions, any charge collected by the dust particle is averaged over its entire surface. For a dielectric dust particle, $E_{||}$ may be finite and so $\sigma(\Theta)$ is not necessarily constant. To allow for nonuniform charging of the dust particle, we additionally solved a continuity equation for the surface charge,

$$\frac{\partial\sigma(\Theta)}{\partial t} = \nabla_\Theta \cdot \mu_s \vec{E}(\Theta)\sigma(\Theta) + S(\Theta) \tag{2}$$

where S is the source of surface charge due to collection of electrons and ions from the plasma, and μ_s is an effective

surface mobility for the surface charges. ∇_Θ denotes the tangential component of the gradient operator. We found that for $\mu_s \geq 1\,\mathrm{cm}^2/V-s$, the surface charge becomes essentially uniform as a function of position in less than 1 ns. Most dielectric spherical particles whose diameter $d < E/\nabla E$ (E is the bulk field) will therefore behave like conductors since E_Θ is strong enough to homogenize the charge distribution for any reasonable μ_s. In any event, particles which rotate (even if dielectric) will collect charge homogeneously.

Collisions of pseudoelectrons with heavy particles are included in the PCC/MCC simulation using standard Monte Carlo algorithms. All applicable elastic, inelastic, ionization and attachment collisions are included. A modified null cross section technique was employed in the manner described in detail in [26]. When either an electron or ion pseudoparticle collides with the dust particle, it is removed from the simulation and its charge added to the dust particle. Although the capability exists to include secondary electron emission from the surface of the dust particle for either electrons or ions, we did not use this option for the results presented here.

The ion MCC portion of the model is conceptually the same as that for electrons. Three classes of collisions for ions were included; elastic (with neutrals), charge exchange (with neutrals) and coulomb (with other ions). The ion-ion coulomb collisions were incorporated into the model in the same manner as electron-electron collisions as described in [26]. Briefly, when initially formulating the ion collision frequency for use in the MCS, an estimate of the maximum ion density N_{IM} is made. This value is used for computing the ion-ion collision frequency. During the simulation, statistics are gathered on the ion density as a function of position, $N_I(r, \Theta)$. If an ion-ion collision is selected in the MCS, another random number ($r = (0, 1)$) is chosen. If

$$r \leq \frac{N_I(r, \Theta)}{N_{IM}}, \tag{3}$$

then an ion-ion collision is said to occur. Using this method, vector information on the ion collision partner is not available. We instead assume that all ion-ion collisions are isotropic.

For typical plasma densities ($10^{10} - 10^{11}\,\mathrm{cm}^{-3}$) and shielding lengths (a few to tens of μm), the number of ions in the shielding volume is only tens to hundreds. For these conditions, the simulation is sensitive to the number of ions (electrons) that each pseudoparticle represents. For example, the calculated particle potential becomes more negative as the ions (electrons) per pseudoparticle decreases towards one. This effect is presumably due to the coarse representation of positive charge in the shielding volume. In practice, we operated with one pseudoparticle representing one ion (electron) resulting in the use of 20,000–120,000 particles. If one uses this scaling, then the "noise" in the simulation approximates real statistical fluctuations. As a side point, when simulating low plasma densities, there is an upper limit to the number of particles which can be used since we chose not to have pseudoparticles represent a fractional number of ions (electrons). This choice differs from that used by Boeuf who allowed his pseudoparticles to have different weightings and, in some cases, to have fractional weightings [25].

The simulation was performed in one of two modes. In the first, the dust particle is introduced with zero charge on its surface. The simulation is then simply integrated forward in time until the total charge on the particle, Q, reaches a steady state. This is, unfortunately, a computer intensive process. In the second method, the dust particle is introduced with an initial charge, Q_o, and the corresponding number of electrons is removed from the control volume to insure charge neutrality. The simulation is run long enough to calculate dQ/dt. If $dQ/dt > 0$, then the simulation is restarted with a less negative Q_o. Similarly, if $dQ/dt < 0$, the simulation is started with a more negative Q_o. The process is repeated, interpolating previous values of Q_o, to seek the value of Q_o which results in $dQ/dt = 0$. In either case, we must always have the total net charge in the computational volume (electrons, ions and dust particle) be zero. This is insured by appropriate choice of initial conditions, periodic boundary conditions and conservative collisional kinetics.

Following updates of the electrical potential after collection of charge on the dust particle, we observed numerical heating of both electrons and ions. This effect most likely resulted from the fact that the charge collected on the dust particle is, for all practical purposes, uniformly distributed over the surface. Charge which, for example, was collected from one azimuthal location would, on the next time step, be "felt" by ions (electrons) at all azimuthal locations. Although the numerical heating is not an issue in the quasi-steady state, it is of concern in the relaxation to the steady state when Q is rapidly changing. We treated the numerical heating of pseudoparticles by calculating the total energy (kinetic and potential) prior to and after collection of charge (and update of the potential). We then slightly displaced the pseudoparticle to a larger (smaller) radial position to insure that its energy was conserved. This correction became unnecessary as dQ/dt approached zero.

The two dominant forces on the particle are electrostatic and ion drag. The latter force can be directly calculated in the following fashion. When a steady state charge and density configuration is obtained, a series of test ion pseudoparticles are launched from the borders of the computational volume. The change in momentum of the test particles as they recross the borders of the computational volume is calculated. On the average, the "lost" momentum is transferred to the dust particle, and constitutes the ion drag force.

To incorporate the effects of dust into more global models of contaminated glow discharges, two approaches can be taken. The first fully resolves the electron- (and ion-) dust particle interaction in the manner described here. This technique is computationally taxing since the spatial scales of interests span from less than 1 μm to many centimeters. The second technique is to include the electron- (and ion-) dust particle interaction in the same manner as electron-atom interactions using cross sections. In this regard, there are two cross sections which must be defined. The first is a momentum transfer cross section and the second is an electron (or ion) loss cross section for collection by the dust particle. The latter cross section is analogous to attachment (for electrons) or ion-ion recombination (for ions).

The electron and ion momentum transfer cross sections, and particle loss cross sections were calculated in the same fashion as that for the ion drag force. After completion of the simulation, test ion (or electron) pseudoparticles were directed towards the dust particle with a fixed momentum and incrementally selected impact parameters, b. (Typically 5000 impact parameters between $b = 0$ and the outer radius of the sheath were used). In practice, test trajectories were launched from only a single face of the cubic computational volume. We defined the momentum transfer cross section at a particular energy as

$$\sigma_m(\epsilon) = \sum_i \frac{|\Delta\vec{\nu}|}{|\vec{\nu}_i|} 2\pi b_i \Delta b \tag{4}$$

where $\vec{\nu}_i$ is the initial momentum of the pseudoparticle for impact parameter b_i and $\Delta\vec{\nu}$ is the change in momentum of the pseudoparticle. The momentum of the pseudoparticles which are collected by the dust particle are not included in (4) in accordance with conventions adopted in swarm theory. For example, the contributions of electrons which attach during a swarm experiment are not included in the calculation of the swarm averaged drift velocity and mobility other than by the absence of their trajectories in phase space. The collected ion (electron) pseudoparticles are included in the loss cross section.

The ion (or electron) loss cross section is defined as

$$\sigma_1(\epsilon) = \sum_i \delta_i 2\pi b_i \Delta b \tag{5}$$

where δ_i is one or zero depending upon whether the pseudoparticle is collected or not.

A basic question which must be addressed is whether a PIC simulation is a valid modeling technique for conditions where the charge density is sparse and noncontinuous near the dust particle. A molecular dynamics (MD) simulation accounting for pairwise interactions between all charged particles may be a more appropriate vehicle and might provide a more realistic representation of statistical fluctuations. The good agreement obtained between these techniques [27] and the semianalytic results of Kilgore *et al.* [20] may, in fact, result from the same assumption of quasi-continuous charge distributions inherent in the theory and expected in PIC simulations. Although a side-by-side comparison of a fully self-consistent MD simulation with a PIC/MCC simulation is called for, it is beyond the scope of the present effort.

III. Dynamics of Particle Charging

In this section, the dynamics of dust particle charging will be discussed using results from our model. The total electron and ion charges (in units of 1.6×10^{-19} C) collected by the dust particle (radius 0.5 μm) and the electric potential on the particle are shown in Fig. 2 as a function of time. The gas pressure is 0.2 torr of Ar, the bulk plasma density is $3 \times 10^{11}\,\mathrm{cm}^{-3}$ and the applied E/N is $30 \times 10^{-17}\mathrm{V} - \mathrm{cm}^2$, generating an electron temperature of 3.8 eV far from the dust particle. Note that electrons are collected immediately upon the start of the simulation, a consequence of their larger thermal

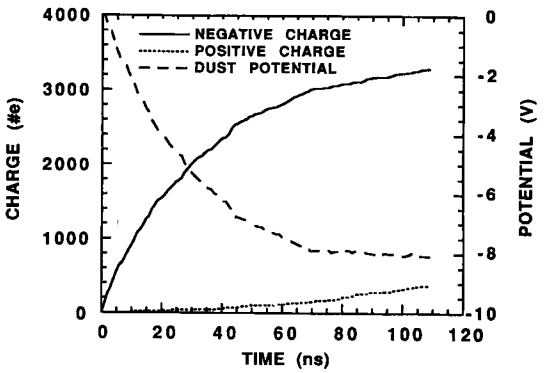

Fig. 2. Time evolution of potential (relative to the bulk plasma) on a 1 μm diameter dust particle, negative charges collected by the dust particle and positive charges collected by the particle. The bulk plasma density is $3 \times 10^{11}\mathrm{cm}^{-3}$. The steady state is reached when the rates of collection of electrons and ions are equal.

flux. A short induction time (10 ns) is required for the sheath to grow and before ions are collected in significant numbers. A steady state is achieved when the rate of collection of electrons and ions is the same; and occurs at $\simeq$70 ns. The equilibration time decreases with increasing plasma density and decreasing electron temperature.

The final net charge on the particles is $Q \approx -3000\,q$, providing a potential of the dust, relative to the bulk plasma potential far from the particle, of -8.1 V, which is approximately $-2.1 \cdot T_e$. This potential is commensurate to, but slightly less than the value one would calculate for a dust particle immersed in a plasma having a Maxwellian electron energy distribution. The potential given by orbital motion limited (OML) theory [16], [21] is $-2.42 \cdot T_e$ or -9.2 V. The reason for this difference most likely results from the forms of out particle distributions. Our EED is "cut-off," meaning that it is depleted of high energy electrons above the inelastic threshold energy (12 eV for argon) relative to a Maxwellian of the same average energy. Recall that the purpose of the particle potential is to reduce the flux of energetic electrons collected on the dust to that value which balances the ion flux. The cut-off EED obtained in real plasmas is depleted of high energy electrons and therefore a smaller potential is required to retard the electron flux to that value which balances the ion flux [28].

The equivalence of our two methods of solution is shown in Fig. 3 where Q is shown as a function of time for three values of Q_o; less negative, equal to, and more negative than the steady state value. Using this "predictor-corrector" technique, the same charge on the particle is calculated as using the fully time dependent calculation. Note that the net charge on the particle fluctuates in time. Since the number of ions (electrons) per pseudoparticle is unity for these conditions, a component of this "noise" represents actual statistical fluctuations. These fluctuations will be discussed in more detail below.

We have found that the charging time of the dust particle increases with increasing electron temperature (obtained by varying E/N) and decreases with increasing diameter and electron density. This scaling can be explained in the following fashion. For otherwise constant conditions, the dust potential is proportional to the electron temperature and scales as Q/d.

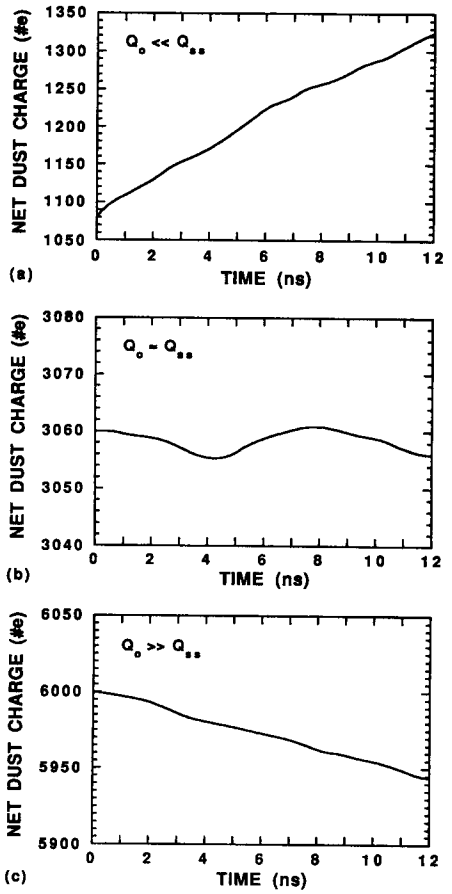

Fig. 3. Examples of the predictor-corrector method of obtaining the number of (negative) charges on a dust particle for the conditions of Fig. 2. These examples show the time evolution of the charge on the particle when the initial number of charges (Q_o) are a) less than, b) equal to and c) greater than the steady state value, Q_{ss}.

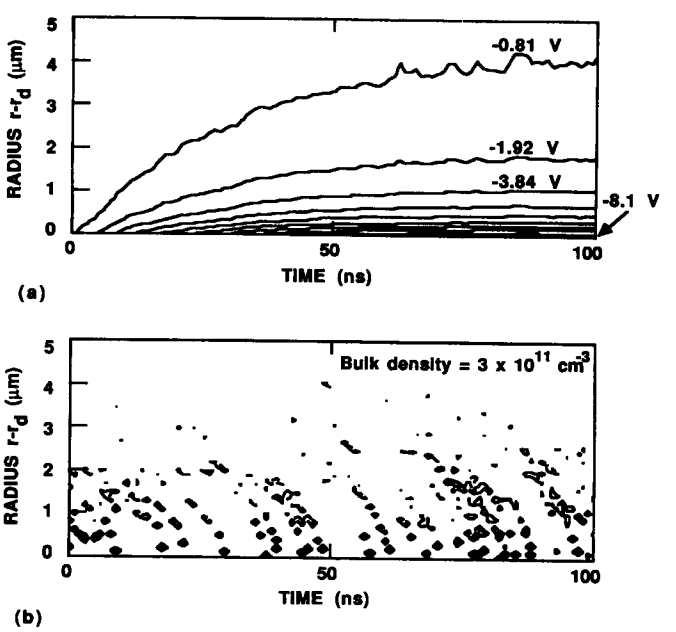

Fig. 4. Evolution of the a) plasma potential and b) ion density as a function of radial distance from the surface of the dust particle (averaged over azimuthal angle) and time for the conditions of Fig. 2. The ion density shows discrete ions (higher density) being swept towards the particle as the sheath expands into the plasma.

For a random electron flux $f \sim T_e^{1/2} n_e$, so $Q \sim f 4\pi d^2 \Delta t$ where Δt is the charging time. Solving for Δt, we obtain $\Delta t \sim T_e^{1/2}/(n_e d)$. Small dust particles charge slowly because they are small targets. Dust particles in hot plasmas charge slowly because the final potential is large. Dust particles in dense plasmas charge quickly because the random electron flux is large.

The scaling of charging times in this fashion has important implications in RF discharge processing plasmas. In low density plasmas ($n_e \ll 10^{10}\,\mathrm{cm}^{-3}$) the charging time is commensurate or longer than the RF cycle (100 s ns). Therefore the charging and shielding of the particle, (and as a result the electron- and ion-dust cross sections) do not vary during an RF cycle. In high density plasmas ($n_e \gg 10^{10}\,\mathrm{cm}^{-3}$), the charging time for the dust particle is less than the RF cycle. Therefore, electron and ion interaction cross sections with the particle will vary during the RF cycle.

The dynamics of the formation of the sheath around the dust particle are shown in Fig. 4 where the electric potential and ion density are shown as a function of radius and time. (The results have been averaged over the azimuthal angle). The sheath thickness is quickly established after the short induction time, and grows only slowly thereafter. The electric potential appears to reach a steady state at small radii at earlier times than large radii. We attribute this to the fact that the potential at small radii is largely determined by the charge and the diameter of the particle. The potential at large radii is determined in larger part by ion dynamics and orbiting. This is apparent from Fig. 4(b) where ions are discretely accumulated by the advancing sheath at successively later times.

The quasi-steady state electron and ion densities are shown in Fig. 5, and quasi-steady state potential is shown in Fig. 6. The densities are shown for both averaged and instantaneous values. Recall that for these conditions each pseudoparticle represents a single electron or ion. Near the particle surface not all computational bins are occupied with ions or electrons. The observed noise may then represent actual statistical fluctuations. The electron density is depressed in the vicinity of the dust particle, a consequence of its negative potential. The ion densities increase in the vicinity of the particle, in this example to a peak averaged density of six times the bulk density far from the particle. The increase in the ion density is a consequence of the open and closed orbits of ions around the dust particle which, as a result of the decrease in radial velocity, increases the density. The orbital component of the ion motion decreases as λ/d (shielding distance/dust particle diameter) decreases; and for these reasons the increase in the ion density in the vicinity of the particle decreases with decreasing λ/d. Peak ion densities near the dust particle as a function of diameter of the dust particle showing this scaling appears in Fig. 7. (The bulk ion density is $3 \times 10^{10}\,\mathrm{cm}^{-3}$). For a given surface charge density, this tends to increase the shielding length with decreasing λ/d. These simulation results agree fairly well with the semianalytic theory of Daugherty *et al.* [21].

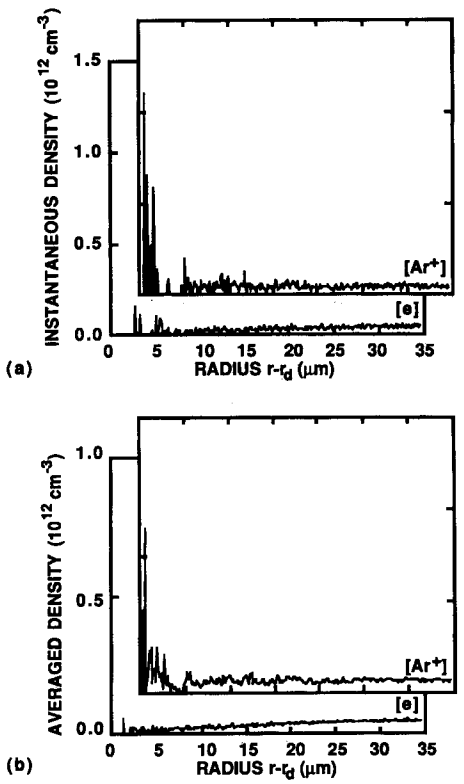

Fig. 5. Electron and ion densities as a function of distance from the surface of a 1 μm dust particle for a bulk plasma density of 3×10^{11} cm^{-3}. a) instantaneous values and b) values averaged over five successive time steps. The electron density decreases inthe negative potential surrounding the particle while the ion density increases due to orbital motion around the dust particle. The noise in the densities near the particle are representative of real statistical fluctuations since each pseudoparticle represents one electron or ion.

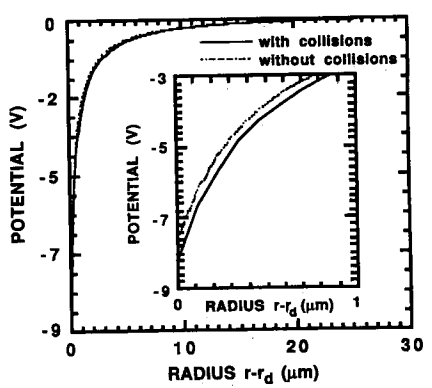

Fig. 6. Instantaneous snapshot of the plasma potential around a particle for the conditions of Fig. 5. Potentials are shown when including and excluding charge exchange collisions.

The shielding distance in Fig. 6, defined as the radius at which the magnitude of the potential falls to 0.1 of its maximum value, is $\simeq 3.5\,\mu$m. The precise shielding distances fluctuates slightly due to the statistical fluctuations of the ion charge in the shielding volume and the fluctuations in the charge on the particle. The potential profile shown in Fig. 6 is an instantaneous snapshot. The shape of our potential is broader than that predicted by Daugherty *et al.* [21] if we equate the ion temperature with their monoenergetic ion energy ($T_e = 3.8\,\text{eV}, T_I = 0.026$ eV). The semianalytic theory of

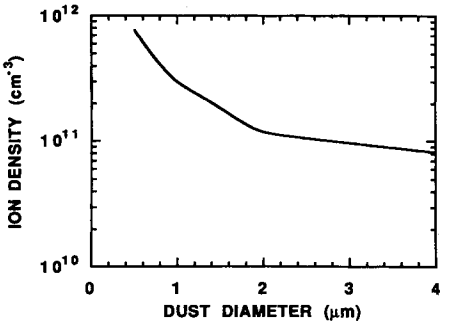

Fig. 7. Ion density near the surface of a 1 μm dust particle as a function of the diameter of the dust particle. The bulk plasma density is $3 \times 10^{10}\text{cm}^{-3}$. The ion density increases near the particle due to an increase in the orbital component of the ion motion.

Daugherty *et al.* [21] is fit well by a Debye-Huckel potential using a linearized Debye length except at large radii. The Debye-Huckel potential is $\phi(r) = \phi(a)(a/r) \cdot \exp(-(r - a)/\lambda_L)$, where a is the radius of the dust particle, λ_L is the linearized Debye length ($\lambda_L^{-1} = (q^2 N/\epsilon_o \cdot (1/kT_e + 1/2E_o))^{1/2}$), and E_o is a monoenergetic ion energy. Our potential does not fall as rapidly as the Debye-Huckel at radii smaller than λ_L. We suspect this difference may result from the non-monoenergetic distribution of ion energies in our simulation and the non-continuum distribution of our ion particles.

The results of Boeuf [25] differ somewhat from ours in that his floating potentials are only a small fraction of the electron temperature. These results are a consequence of the fact that the dust density in his simulations is sufficiently large that the dominant loss of plasma is by electron-ion recombination on their surface, and a large fraction of the negative charge in the plasma resides on the dust.

The ion density increases near the dust particle due to open and closed orbits. The large increase in ion density near the particle resulting from closed orbits shrinks the shielding length. Closed orbits occur when an ion has a collision in the sheath region, reducing the net momentum of the particle and dropping it into an orbit. These ions are often subsequently collected when they undergo another collision, or may be "kicked" out of orbit by collisions which increase their momentum. Although the majority of ions undergo collisionless open orbits, we have chosen a representative sampling of ion orbits around a $4\,\mu$m dust particle during which collisions occur; and these are shown in Fig. 8. The 3-D trajectories are shown as 2-D projections in the figure. Trajectory (a) is an open orbit. The ion undergoes two collisions. The first collision is a backscattering elastic collision with directs the ion into a different open orbit. The ion of trajectory (b) experiences a charge exchange collision on its outbound journey. The loss of momentum resulting from the collision allows the new ion to be collected by the particle. Trajectory (c) shows an ion which, after having a collision, falls into a closed orbit for a few cycles, and then experiences a second collision which "kicks" it into an open orbit. The ion in trajectory (d) suffers a glancing collision which drops it into a precessing orbit, similar to that described by Goree [27].

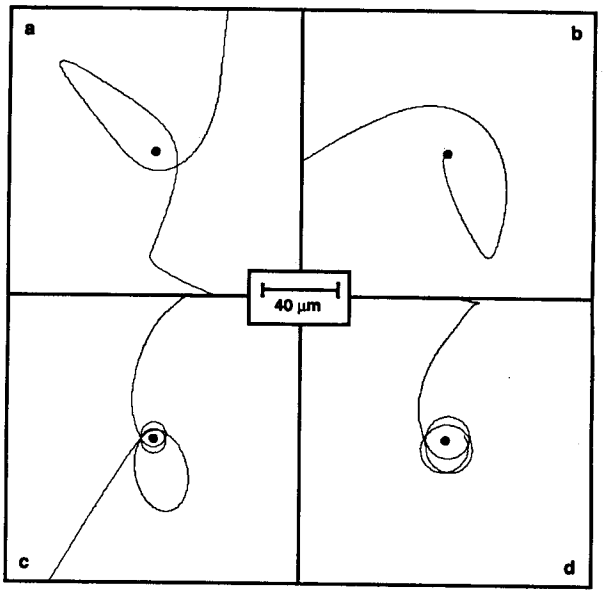

Fig. 8. Representative collisional ion trajectories around a 4 μm diameter dust particle in 200 mtorr of Ar. The trajectories represent a) open orbiting, b) collection following a charge exchange collisions, c) closed orbiting with a "kick-out" collision and d) precessing closed orbiting.

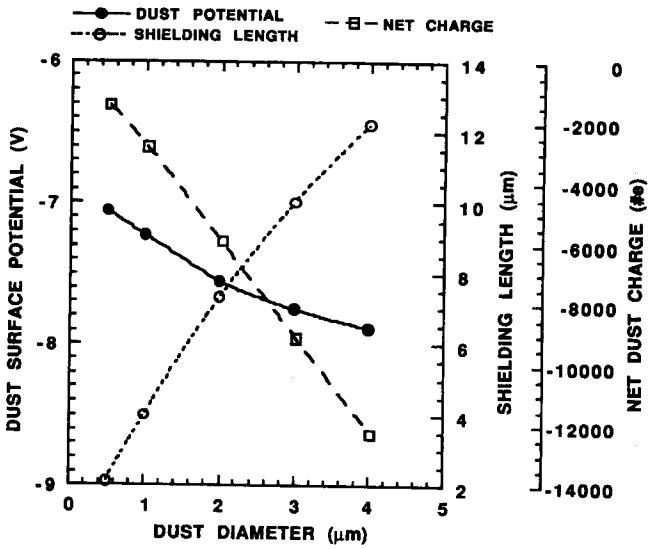

Fig. 9. Particle potential, shielding length and net number of elementary charges on the surface of the dust as a function of dust diameter ($[e] = 3 \times 10^{10}\text{cm}^{-3}, T_e = 3.8$ eV). The potential becomes more negative and charges increase with increasing diameter as the ratio λ/d decreases.

The occurrence or absence of collisions can affect the potential and shielding of the particle. For example, dust potentials are shown in Fig. 6 when ions have and do not have charge exchange collisions. Without charge exchange collisions, the ion temperature is higher, and therefore the flux of ions randomly collected by the particle increases. This results in an increase in the potential of the dust particle (to a less negative value). One must, however, be cautious in assessing the effect of ion collisions on the particle potential. We have observed both increases and decreases in the potential of the dust particle when including, or excluding, collisions. For example, when λ is larger than the ion mean free path, charge exchange collisions allow ions to more readily fall into the dust particle, and so the dust potential becomes less negative.

The dust potential (relative to the bulk plasma), the total charge on the dust particle and the shielding distance are shown in Fig. 9 as a function of diameter of the dust particle. In the limit of large dust particles ($d \gg \lambda$), the surface appears to be macroscopically large and the sheath potential approaches the floating potential of a large isolated body. For sufficiently small particles ($d \ll \lambda$) there is little, if any, shielding required. Our simulations show an increase (to more negative values) of the dust potential in going from particle sizes of 0.5 to 4.0 μm diameter (-7.1 V to -7.8 V). Over this range of particle sizes, λ/d decreases from 4 to 3. The total charge on the particle scales roughly with the diameter. The semianalytic results of Daugherty *et al.* [18] show similar trends.

The potential on the dust, the net charge and shielding length are shown in Fig. 10 as a function of electron temperature, T_e. The electron temperature was varied by changing the externally applied E/N. Therefore, there is also a small increase in ion temperature with increasing T_e. The dust potential becomes more negative, as does the charge on the dust particle, with increasing T_e since the random flux of high energy electrons also increases. Since, however, the shielding distance is best described by the linearized Debye length, which is a weak function of T_e, the shielding length does not appreciably change. At low electron temperatures, we see an increase in the shielding length with increasing T_e, a consequence of the contribution of T_e to the linearized Debye length. This trend reverses at large T_e. Although this result is reproducible, it is difficult to explain, and may result from an increase in plasma density during the simulation resulting from a larger rate of ionization at the higher electron temperature.

We also computed the surface potential, the net charge, and shielding length as a function of the ion density, as shown in Fig. 11. As the plasma density increases the shielding length decreases as one would expect by the decrease of λ_L with increasing plasma density. However, the computed surface potential decreased (to more negative values) by as much as a volt with increasing plasma density ($<10^{10}\,\text{cm}^{-3}$ to $10^{11}\,\text{cm}^{-3}$). This trend was also observed by Boeuf [22]. The periodic boundary conditions used in our simulation provide a computational cell of $120\,\mu\text{m}^3$ which implies a dust particle density of $5.8 \times 10^5\,\text{cm}^{-3}$. For a plasma density of $1 \times 10^{11}\,\text{cm}^{-3}$ there are $\simeq 173,000$ electrons in the volume. With a $1\,\mu$m dust particle having $\simeq 2000$ charges, approximately 1% of the charge resides on the dust particle, which depletes the electrons in the bulk plasma. This reduces the flux of electrons to the dust particle. The results in Fig. 11 can be explained by this "depletion" effect which occurs when significant charge resides on the dust particle.

The depletion of mobile negative charge in the plasma as a consequence of charging of dust particles, and its role in increasing the particle potential, was addressed by Havnes *et al.* in the context of space plasmas [29]. Havnes derived a

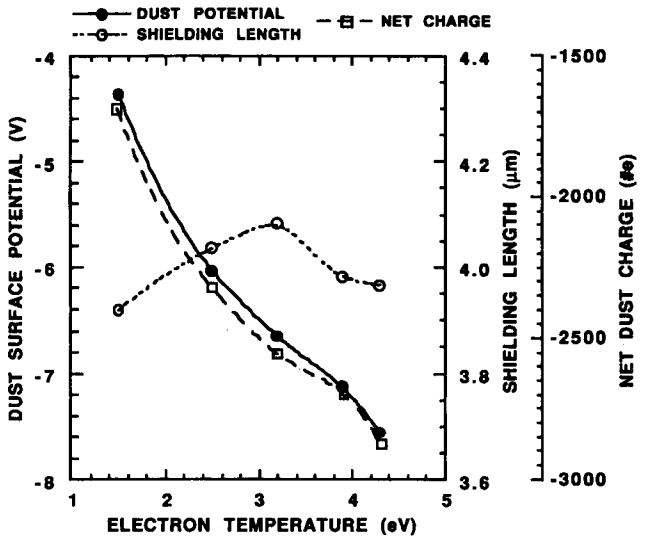

Fig. 10. Particle potential, shielding length and net number of elementary charges on the surface of the dust as a function of electron temperature ($d = 1\,\mu$m, $[e] = 3 \times 10^{10}\,\mathrm{cm}^{-3}$). The electron temperature was varied by changing the E/N of the bulk plasma. The potential becomes more negative and the shielding mildly increases with increasing electron temperature.

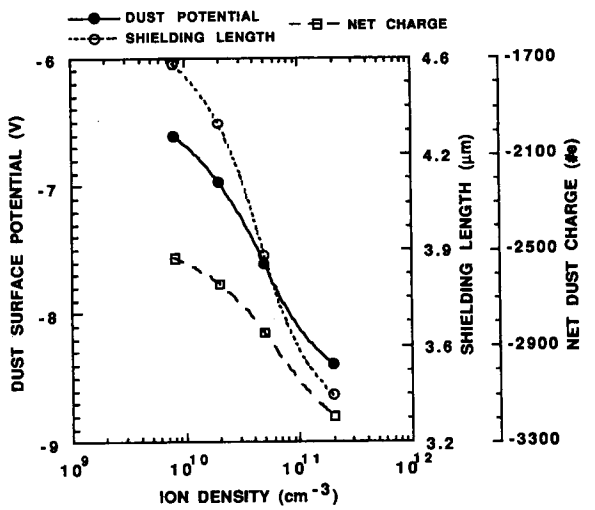

Fig. 11. Particle potential, shielding length and net number of elementary charges on the surface of the dust as a function of ion density. The shielding length increases with decreasing plasma density due to the lengthening of λ_L. The potential becomes more less negative and with decreasing plasma density due to a depletion of electrons in the bulk plasma which reduces the electron flux. The effective dust particle density is $\simeq 5 \times 10^5\,\mathrm{cm}^{-3}$.

parameter:

$$P = \frac{N_D a T}{N} \tag{6}$$

where N_D is the dust density, a is the radius of the dust particle (m), T is the plasma temperature (eV) and N is the plasma density (m^{-3}). When P is small ($P < 10^{-13}$), the particle can be considered isolated. When P is large ($P > 10^{-12}$), significant charge resides on the dust particles, and the particle potential becomes less negative. This result can be applied to our conditions by appropriately modifying the orbital motion limited theory.

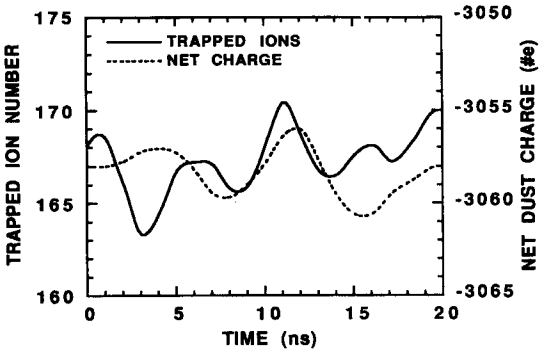

Fig. 12. The net charge on a dust particle and the number of trapped orbital ions as a function of time ($[e] = 3 \times 10^{11}\,\mathrm{cm}^{-3}$, $d = 1\,\mu$m, $T_e = 3.8$ eV). These quantities fluctuate due to the statistically small number of ions in the shielding volume at any given time.

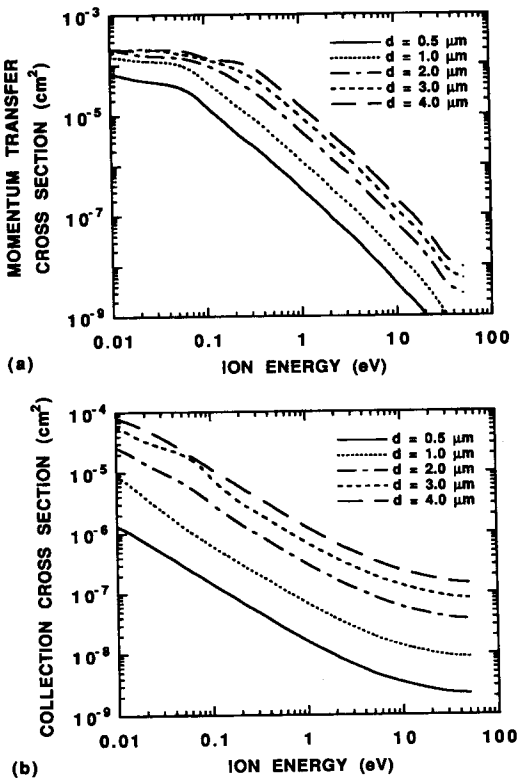

Fig. 13. Ion-dust cross sections for a) momentum transfer and b) collection as a function of ion energy for various dust diameters ($[e] = 3 \times 10^{10}\mathrm{cm}^{-3}, T_e = 3.8$ eV). These cross sections generally increase with increasing dust diameter. The asymptotic collection cross section is simply the geometrical cross section of the dust particle.

The orbital motion limited (OML) theory states that the particle potential should be independent of plasma density [16], [21]. Using OML, the particle potential ϕ is determined by balancing the current of electrons (I_-) and ions (I_+) to the dust

$$I_+ = \pi a^2 N_+ \left(\frac{2E_o}{M}\right)^{1/2} \left(1 - \frac{q\phi}{E_o}\right) \tag{7a}$$

$$I_- = \pi a^2 N_- \left(\frac{8kT_e}{\pi m}\right)^{1/2} \exp\left(\frac{q\phi}{kT_e}\right) \tag{7b}$$

where N is the bulk electron or plasma density, a is the radius of the dust particle, E_o is the ion energy (assumed monoenergetic), M is the ion mass and m is the electron mass. Defining $\chi = q\phi/kT_e$, the particle potential can be obtained by solving,

$$1 = \left(\frac{N_-}{N_+}\right)\frac{\exp(\chi)}{\left(1-\chi\frac{kT_e}{E_o}\right)}\left(\frac{M4kT_e}{\pi m E_0}\right)^{1/2} \tag{8}$$

which equates the flux of negative and positive charges to the dust particle. This formulation assumes that the volume density of dust particles, ρ_D, is sufficiently small that the total negative charge on the dust, $\rho_D Q \ll N_+$. If that is the case, $(N_-/N_+) = 1$ and ϕ is independent of plasma density. However, if $\rho_D Q/N_+$ is not negligible then N_- is reduced and the current of electrons to the dust particle is also commensurately reduced. This "depletion" effect results in an increase (to more positive values) of ϕ as $\rho_D Q/N_+$ increases since the flux of energetic electrons decreases relative to the ion flux.

One can estimate the depletion effect by noting that,

$$\frac{1}{4\pi\epsilon_o}\frac{qQ}{a} \simeq \phi, \qquad Q \simeq \chi\cdot\left(\frac{kT_e}{q^2}\right)4\pi\epsilon_o. \tag{9}$$

With the available electron density being reduced by $\rho_D Q$ in a dusty plasma, the ratio (N_-/N_+) in (8) should be replaced by

$$\left(\frac{N_-}{N_+}\right) \rightarrow 1 + \left(\frac{\rho_D}{N_+}\right)\cdot\chi\cdot\left(\frac{kT_e}{q^2}\right)4\pi\epsilon_o. \tag{10}$$

We used this value for (N_-/N_+) in (8) and calculated ϕ for parameters typical of our plasmas ($T_e = 3.8\,\text{eV}$, $E_o = 0.03\,\text{eV}$, $a = 1\,\mu\text{m}$). We found that ϕ = –9.2 V for $\rho_D/N_+ = 0$, and that ϕ increases to –7.9 V for $\rho_D/N_+ = 7\times10^{-5}$. This corresponds to $\rho_D = 10^6\,\text{cm}^{-3}$ and $N_+ = 1.4\times10^{10}\,\text{cm}^{-3}$, which are commensurate with results from our simulation. According to the Havnes theory, $P = 10^{-10}$, which would imply an increase in particle potential to ≈–2.9 V.

One convenient feature of our simulations is that the each pseudoparticle represents a single electron or ion, and hence one may approximate statistical fluctuations in the charge collection and shielding properties. Examples of these fluctuations are seen in Fig. 12 where the total charge on the particle is plotted as a function of time. These fluctuations roughly correlate with the statistical fluctuations in the number of ions in the shielding volume, and therefore represents the maximum fluctuation in the rate of collection of ions. For example, for a bulk plasma density of $3\times10^{11}\,\text{cm}^{-3}$ and shielding length of $5\,\mu\text{m}$, there are approximately 160 ions in the shielding volume. This results in a statistical fluctuation of 12 ions in the shielding volume, whereas the net charge fluctuates with a peak-to-peak amplitude of ≃5.

Ions undergoing closed orbits around the dust particle are trapped in the potential well of the particle. The definition of a trapped ion is when the sum of its effective potential energy (including an angular momentum correction) and kinetic energy is negative [26]. As an approximation, we calculated the total number of trapped ions as a function of time using as a trapping criterion that $q\phi+1/2mv^2 < 0$. The results are shown in Fig. 12. Approximately 165–170 ions are trapped at any given time, with their numbers fluctuating with an amplitude of 5. The trapped positive charge represents ≃5–6% of the total charge on the dust particle. The number of trapped ions shown here is commensurate to one that would be obtained by extending the theory of Goree to plasma processing conditions [29].

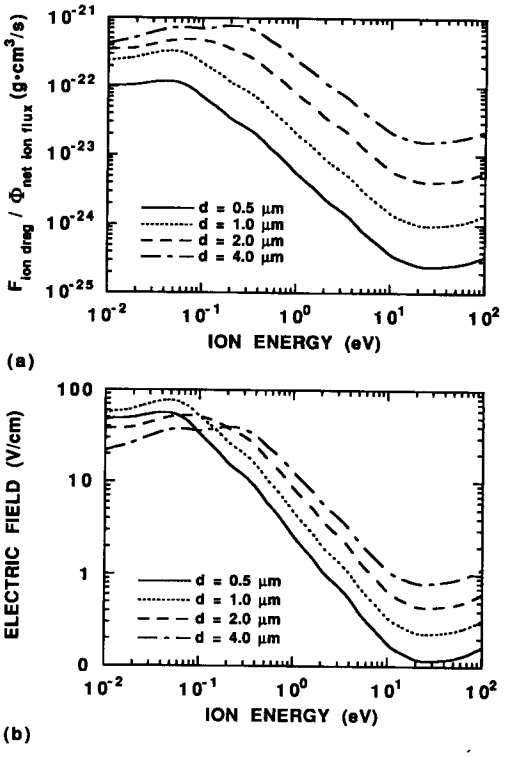

Fig. 14. Calculated parameters relating to the ion drag force on a dust particle. a) ion drag (divided by ion flux) for various dust diameters ($[e] = 3\times10^{10}\text{cm}^{-3}$, $T_e = 3.8$ eV). b) Electric field which generates an electrostatic force balancing the ion drag force. The ion flux is $\phi = 10^{15}\text{cm}^2\text{s}^{-1}$. The increase in the ion drag force with increasing dust diameter in part explains why larger particles accumulate deeper in the sheath.

IV. Ion- and Electron-Dust Interaction Cross Sections

Ion-dust cross sections for collection and momentum transfer are shown in Fig. 13 as a function of ion energy for various dust diameters. These cross sections were obtained with the molecular dynamics simulation using the potentials calculated in the PIC/MCC simulation. The bulk plasma density and electron temperature are constant ($3\times10^{10}\,\text{cm}^{-3}$, $T_e = 3.8$ eV). The collection cross section decreases with increasing ion energy, as the kinetic energy of the ion approaches the magnitude of the particle potential. When the ion energy exceeds the magnitude of the particle potential, the collection cross section is essentially the geometrical cross sectional area of the dust particle. As a result, the collection cross sections increase with increasing diameter of the dust particle in proportion to the cross sectional area of the particle. The ion-dust momentum transfer cross section (exclusive of collected ions) is relatively flat at low ion energies (below 0.1 eV) and

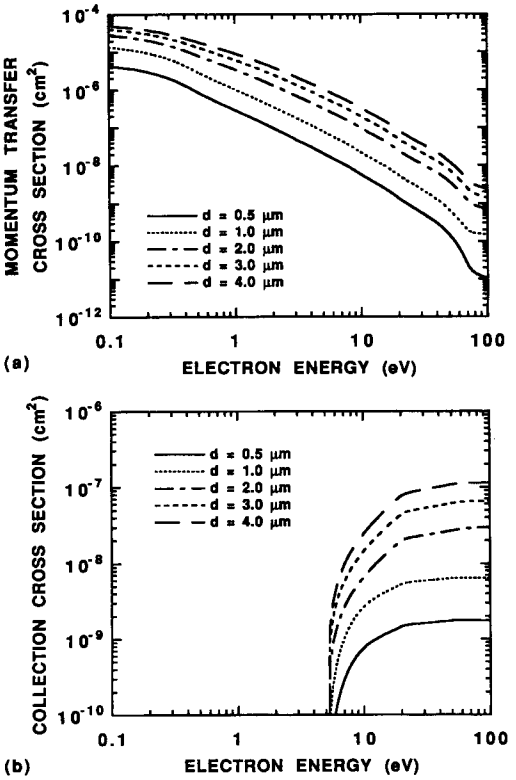

Fig. 15. Electron-dust cross sections for a) momentum transfer and b) collection as a function of electron energy for various dust diameters ($[e] = 3 \times 10^{10}\mathrm{cm}^{-3}, T_e = 3.8$ eV). These cross sections generally increase with increasing dust diameter. The collection cross section is zero for energies below the dust potential. The asymptotic collection cross section is simply the geometrical cross section of the dust particle.

decreases with increasing ion energy roughly as $1/\epsilon^{1.8}$. These results agree well with the semianalytic theory of Kilgore *et al.* [20].

The ion drag force (normalized by the total ion flux) as a function of ion energy is shown in Fig. 14(a). The total ion drag force on the dust particles is obtained by summing the contributions from momentum transfer resulting from open ion orbits, as represented by the cross section in Fig. 13(a), and from direct collection, as represented by the cross section in Fig. 13(b);

$$\vec{F}(u) = [Mu(\sigma_m + \sigma_c)]\vec{\phi}(u) \tag{11}$$

where M is the ion mass, u is its speed and ϕ is the net ion flux. At low ion energies, the momentum transfer cross section is a weak function of energy. Therefore, increasing ion energy results in an increase in the rate of momentum transfer. For ion energies exceeding 0.1 eV, the decrease in the momentum transfer cross section exceeds the increase in the momentum of the ion, and so the ion drag decreases. At energies exceeding 10 eV, the collection cross section, which is insensitive to changes in ion energy in that range, dominates momentum transfer. The ion drag force therefore increases with increasing ion energy. The ion drag is least sensitive to the size of the particle at low ion energies where the momentum transfer cross section is largely determined by the diameter of the shielded region. The ion drag is most sensitive to particle size at high

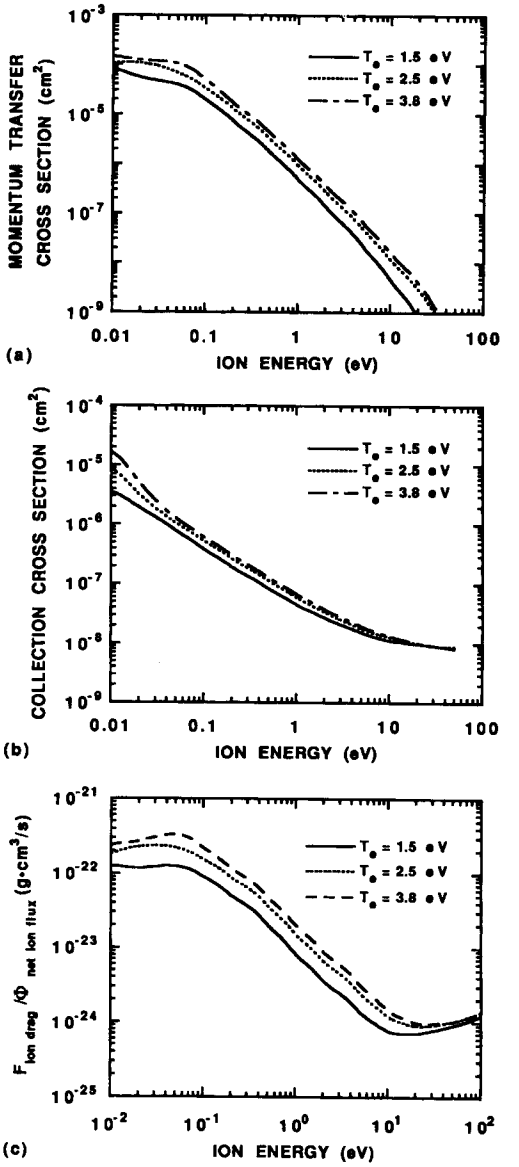

Fig. 16. Ion-dust interaction parameters for various electron temperatures. a) Cross sections for ion-dust momentum transfer as a function of ion energy, b) ion collection cross section as a function of ion energy, and c) ion drag force (divided by ion flux) for the same conditions. ($[e] = 3 \times 10^{10}\mathrm{cm}^{-3}$, $d = 1\,\mu$m). These cross sections generally increase with increasing electron temperature due to a small increase in shielding distance and increase in particle potential.

energy where the total momentum transfer cross section is the geometrical cross section of the particle. This scaling in part explains why larger dust particles accumulate closer to the substrate in glow discharges. The equilibrium point for large particles, subject to a larger ion drag force, is found at a location deeper in the sheath where the electric field is larger. This shape for the ion drag force was predicted by the semianalytic theory of Barnes *et al.* [12].

Particles typically accumulate in RF glow discharges at the edges of sheaths where the electrostatic forces balance the ion drag forces. The electric field which balances the ion drag force (for $\phi = 10^{15}\,\mathrm{cm}^{-2}s^{-1}$, a value typical of RF glow discharges) is shown in Fig. 14(b) as a function of ion energy for different particle diameters. For ion energies greater than

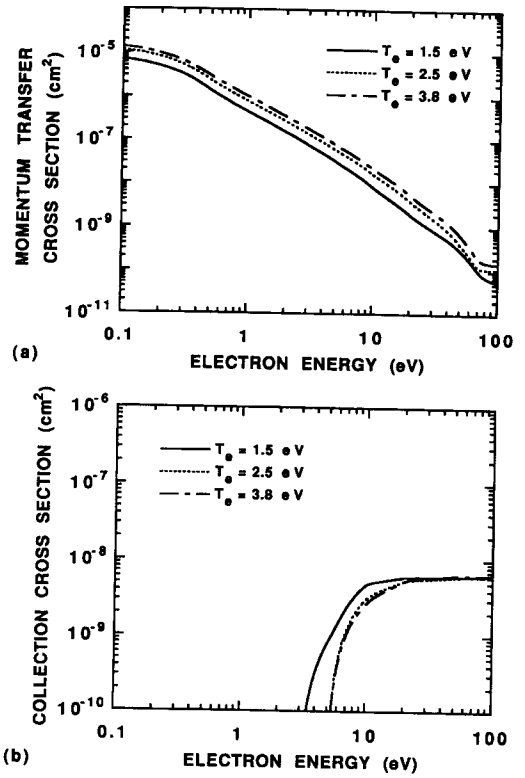

Fig. 17. Electron-dust cross sections for a) momentum transfer and b) collection as a function of ion energy for various electron temperatures ($[e] = 3 \times 10^{10}\text{cm}^{-3}$, $d = 1\,\mu\text{m}$).

0.1 eV, the electric field which balances the ion drag force scales similarly to the ion drag force as a function of both ion energy and particle size. Larger particles suffer more ion drag and require a larger electric field to balance that force. The unshielded charge on the dust particle, however, scales with the size of the particle. At low ion energies where the ion drag forces are less sensitive functions of dust diameter, the electric fields which balance the drag force are commensurate.

The momentum transfer cross section (exclusive of collection) and the collection cross sections for electrons for various dust particle diameters appear in Fig. 15. The momentum transfer cross section decreases with increased electron energy, scaling approximately at $1/\epsilon^{2.4}$. Since the force between the electron and the dust particle is repulsive, the electron collection cross section is zero until the electron energy equals or exceeds the floating potential of the dust particle. In a similar fashion to the ion collection cross section, the asymptotic value of the electron collection cross section correponds to the geometrical cross section of the dust particle.

Ion-dust cross sections and ion drag forces are shown in Fig. 16 as a function of electron temperature for a dust diameter of 1 μm. The electron-dust cross sections appear in Fig. 17 for the same conditions. The qualitative trends for the scaling of the cross sections are the same as discussed above. The momentum transfer and collection cross sections for ions increase with increasing T_e due to the small increase in shielding length resulting from the electron contribution to the linearized Debye length, and due to the increase in the potential of the particle. Since the asymptotic value of the collection cross sections for both electrons and ions depend only on the size of the particle, these values are independent of the electron temperature.

V. Concluding Remarks

A pseudoparticle-in-cell simulation has been developed and used to investigate the shielding properties of dust particles in low temperature plasmas. We found that the simulation was quite sensitive to the number of electrons or ions represented by each pseudoparticle. Systematic errors were introduced if the number of electrons or ions per pseudoparticle greatly exceeded one. Particle potentials and shielding lengths were discussed for dust particles in argon discharges typical of plasma processing. We found that the particle potential is 1.5–2 times the electron temperature, slightly less than that predicted by theories [16], [18], [21]. We attribute these differences to non-Maxwellian electron energy distributions and non-monoenergetic ion distributions which tend to decrease the contribution of high energy electrons and increase the contributions of high energy ions. We found nearly identical properties for dielectric and metallic particles for our conditions due to the large tangential electric fields on the surface of the dielectric particles. We observed both open and closed orbits of ions. For typical conditions, 100–200 ions are in trapped ion orbits (defined as having a negative total energy). The one-to-one correspondence of pseudoparticles and electrons (or ions) allowed fluctuations in the shielding properties of the particle to be approximated. The observed fluctuations in charge on the particle and the number of trapped ions can be correlated with the statistical fluctuations in the number of ions in the shielding volume. We determined that for large values of ρ_D/N_+, the particle potential increases (to less negative values) due to a depletion of electrons. This depletion reduces the electron flux to the dust particle relative to the ion flux.

Ion- and electron-dust momentum transfer and collection cross sections were computed. The momentum transfer cross sections increase with increasing dust diameter and electron temperature. The asymptotic values of the collection cross sections are the geometrical cross section of the dust particle.

Acknowledgment

The authors would like to thank M. Barnes, A. Garscadden, J. Goree, D. Graves, and J. Keller for their advice and discussions on dusty plasmas.

[1] R. M. Roth, K. G. Spears, G. D. Stein, and G. Wong, "Spatial dependence of particle light scattering in an RF silane discharge," *Appl. Phys. Lett.*, vol. 46, pp. 253–255, 1985.

[2] G. S. Selwyn, J. E. Heidenreich, and K. L. Haller, "Particle trapping phenomena in radio frequency plasmas," *Appl. Phys. Lett.*, vol. 57, pp. 1876–1878, 1990.

[3] G. S. Selwyn, J. Singh, and R. S. Bennett, "*In situ* laser diagnostic studies of plasma-generated particulate contamination," *J. Vac. Sci. Technol.*, vol. A7, pp. 2758–2765, 1989.

[4] G. S. Selwyn, J. S. McKillop, K. L. Haller, and J. J. Wu, "*In situ* plasma contamination measurements by HeNe laser light scattering: a case study," *J. Vac. Sci. Technol.*, vol. A8, pp. 1726–1731, 1990.

[5] G. M. Jellum and D. B. Graves, "Particle-plasma interactions in low-pressure discharges," *Appl. Phys. Lett.*, vol. 57, pp. 2077–2079, 1990.

[6] G. M. Jellum and D. B. Graves, "Particulates in aluminum sputtering discharges," *J. Appl. Phys.*, vol. 67, pp. 6490–6496, 1990.

[7] G. M. Jellum, J. E. Daugherty, and D. B. Graves, "Particle thermophoresis in low pressure glow discharges," *J. Appl. Phys.*, vol. 69, pp. 6923–6934, 1991.
[8] Y. Watanabe, M. Shiratani, and H. Makino, "Powder-free plasma chemical vapor deposition of hydrogenated amorphous silicon with high RF power density using modulated RF discharge," *Appl. Phys. Lett.*, vol. 57, pp. 1616–1618, 1990.
[9] Y. Watanabe, M. Shiratani, M. Yamashita, "Observation of growing kinetics of particles in a helium-diluted silane RF plasma," *Appl. Phys. Lett.*, vol. 61, pp. 1510–1512, 1992.
[10] R. N. Carlile, S. Geha, J. F. O'Hanlon, and J. Stewart, "Electrostatic trapping of contamination particles in a process plasma environment," *Appl. Phys. Lett.*, vol. 59, pp. 1167–1169, 1992.
[11] T. J. Sommerer, M. S. Barnes, J. H. Keller, M. J. McCaughey, and M. J. Kushner, "Monte Carlo-fluid hybrid model of the accumulation of dust particles at sheath edges in radio-frequency discharges," *Appl. Phys. Lett.*, vol. 59, pp. 638–640, 1991.
[12] M. S. Barnes, J. H. Keller, J. C. Forster, J. A. O'Neill, and D. K. Coultas, "Transport of dust particles in glow-discharge plasmas," *Phys. Rev. Lett.*, vol. 68, pp. 313–316, 1992.
[13] S. G. Geha, R. N. Carlile, J. F. O'Hanlon, and G. S. Selwyn, "The dependence of contamination particle traps on wafer material and topography," *J. Appl. Phys.*, vol. 72, pp. 374–383, 1992.
[14] L. Boufendi, A. Plain, J. Ph. Blondeau, A. Bouchoule, C. Laure, and M. Toogood, "Measurements of particle size kinetics from nanometer to micrometer scale in a low-pressure argon-silane radio-frequency discharge," *Appl. Phys. Lett.*, vol. 60, pp. 169–171, 1992.
[15] G. S. Selwyn and E. F. Patterson, "Plasma particulate contamination control. II. Self-cleaning tool design," *J. Vac. Sci. Technol.*, vol. A10, pp. 1053–1059, 1992.
[16] C. K. Goertz, "Dusty plasmas in the solar system," *Rev. of Geophys.*, vol. 27, pp. 271–292, 1989.
[17] O. Havnes, G. E. Morfill, and C. K. Goertz, "Plasma potential and grain charges in a dust cloud embedded in a plasma," *J. Geophys. Res.* vol. 89, pp. 10999–11003, 1984.
[18] E. C. Whipple, T. G. Northup, and D. A. Mendes, "The electrostatics of a dusty plasma," *J. Geophys. Res.* vol. 90, pp. 7405–7413, 1985.
[19] J. E. Daugherty, R. K. Porteous, and D. B. Graves, "Electrostatic forces on small particles in low-pressure discharges," *J. Appl. Phys.*, vol. 73, pp. 1617–1620, 1993.
[20] M. D. Kilgore, J. E. Daugherty, R. K. Porteous, and D. B. Graves, "Ion drag on an isolated particulate in a low-pressure discharge," *J. Appl. Phys.*, vol. 73, pp. 7195–7202, 1993.
[21] J. E. Daugherty, R. K. Porteous, M. D. Kilgore, and D. B. Graves, "Sheath structure around particles in low-pressure discharges," *J. Appl. Phys.*, vol. 72, pp. 3934–3942, 1992.
[22] M. J. McCaughey and M. J. Kushner, "Electron transport coefficients in dusty argon plasmas," *Appl. Phys. Lett.*, vol. 55, pp. 951–953, 1989.
[23] M. J. McCaughey and M. J. Kushner, "A model for particulate contaminated glow discharges," *J. Appl. Phys.*, vol. 69, pp. 6952–6961, 1991.
[24] S. J. Choi, M. J. McCaughey, T. J. Sommerer, and M. J. Kushner, "Perturbation of the cathode fall in direct-current glow discharges by particulate contamination," *Appl. Phys. Lett.*, vol. 59, pp. 3102–3104, 1991.
[25] J. P. Boeuf, "Characteristics of a dusty nonthermal plasma from a particle-in-cell Monte Carlo simulation," *Phys. Rev. A*, vol. 46, pp. 7910–7922, 1992.
[26] Y. Weng and M. J. Kushner, "Method for including electron-electron collisions in Monte Carlo simulations of electron swarms in partially ionized gases," *Phys. Rev. A*, vol. 42, pp. 6192–6200, 1992.
[27] S. J. Choi and M. J. Kushner, "Simulation of the shielding of dust particles in low pressure glow discharges," *Appl. Phys. Lett.*, vol. 62, pp. 2197–2199, 1993.
[28] M. J. Kushner, "Floating sheath potentials in non-Maxwellian plasmas," *IEEE Trans. Plasma Sci.*, vol. 13, pp. 6–9, 1985.
[29] O. Havnes, C. K. Goertz, G. E. Morfill, E. Grüm, and W. Ip, "Dust charges, cloud potential and instabilities in a dust cloud embedded in a plasma," *J. Geophys. Res.* vol. 92, p. 2281, 1987.
[30] J. Goree, "Ion trapping by a charged dust grain in a plasma," *Phys. Rev. Lett.*, vol. 69, pp. 277–280, 1992.

Seung J. Choi was born in Kang-won, Korea, in 1964. He received the B.S., M.S., and Ph.D. degrees in electrical engineering from the University of Illinois, Urbana-Champaign in 1988, 1989, and 1993, respectively. During his graduate years, he studied electromagnetism and gaseous electronics. For his Ph.D. thesis, he conducted research in particle generation and contamination problems in the plasma processing of microelectronics under the direction of Prof. Mark J. Kushner.

Currently, he is working for Sandia National Laboratories as a postdoctoral researcher.

Dr. Choi is a member of Tau Beta Pi, Phi Kappa Phi, APS, AVS, and MRS.

Mark J. Kushner (F'91) received the B.A. in astronomy and the B.S. in engineering from the University of California, Los Angeles in 1976. He received the M.S. and Ph.D. degrees in applied physics from the California Institute of Technology in 1977 and 1979, respectively, where he also was a Chaim Weizmann Postdoctoral Research Fellow.

He served on the technical staffs of Sandia National Laboratory, Lawrence Livermore National Laboratory, and Spectra Technology. He joined the Department of Electrical and Computer Engineering at the University of Illinois, Urbana-Champaign in 1986 where he now holds the rank of Professor. He has published more than one hundred refereed papers and presented more than one hundred and seventy conference papers on topics related to plasma processing, dusty plasmas, chemical lasers, pulse power, and laser spectroscopy.

Dr. Kushner is a member of Phi Beta Kappa, Tau Beta Pi, Eta Kappa Nu, the Optical Society of America and the Materials Research Society. He is also a Fellow of the American Physical Society. He has served on the Executive Committees of the Gaseous Electronics Conference, the IEEE Technical Committee on Plasma Science and Applications, and the AVS Plasma Sciences and Technology Division. He is on the editorial board of Plasma Sources Science and Technology and the Transactions on Plasma Science.